Keratin-Based Epidermal Green Autofluorescence is a Common Biomarker of Organ Injury

Mingchao Zhang[1,2], Yujia Li[1,2], Dhruba Tara Maharjan[1], Hao He[1], Yue Tao[1], Danhong Wu[3], Weihai Ying[1,2,#]

[1]Med-X Research Institute and School of Biomedical Engineering, Shanghai Jiao Tong University, Shanghai 200030, P.R. China; [2]Collaborative Innovation Center for Genetics and Development, Shanghai 200043, P.R. China; [3]Department of Neurology, Shanghai Fifth People's Hospital, Fudan University, Shanghai 200240, P.R. China

#: Corresponding author:

Weihai Ying, Ph.D.

Professor, School of Biomedical Engineering and Med-X Research Institute

Shanghai Jiao Tong University

1954 Huashan Road

Shanghai, 200030, P.R. China

E-mail: weihaiy@sjtu.edu.cn

Running head: *Epidermal Autofluorescence is an Injury Biomarker*

Abstract

Human autofluorescence (AF) has shown significant potential for non-invasive diagnosis, while information regarding the pathological implications of the changes of epidermal AF is deficient. Our study has suggested that epidermal green AF may become the first endogenous indicator of the levels of inflammatory and reactive oxygen species (ROS) factors to which the skin is exposed: The AF intensity has virtually linear relationships with the dosages of UV, LPS and ROS in mouse models or skin cell culture studies; and the green AF intensity in skin is also highly correlated with the risk of cerebral small vessel disease patients to develop acute ischemic stroke. Since ROS and inflammatory factors to which healthy skin is exposed should come from such pathways as the blood circulation, epidermal green AF may also become the first biomarker of the levels of oxidative stress and inflammation in the body. We further found that keratin 1 degradation mediates the UV-induced increases in green AF intensity, and that decreased keratin 1 levels can lead to cell death. These findings have collectively suggested that organ damage-produced ROS and inflammatory factors may be transported along the body, producing increased epidermal green AF, which may become a common biomarker for organ injury as well as the levels of inflammation and oxidative stress in the body. Our study has also highlighted an essential relationship between skin's changes and organ damage, as well as critical roles of epidermal keratins in both UV-induced skin damage and non-invasive evaluation of organ injury.

Keywords: Epidermal autofluorescence; Organ injury; Keratin; Oxidative stress; Inflammation.

Introduction

Human autofluorescence (AF) has shown significant promise for non-invasive diagnosis of certain diseases including diabetes [1] and cancer [2]. Melanin, keratins, NADH and FAD are four major known epidermal fluorophores[3,4]. However, there is distinct deficiency in the information regarding the effects of various pathological insults on epidermal AF. Since oxidative stress and inflammation are common key pathological factors in the organ injury of a number of diseases such as acute ischemic stroke (AIS) [5,6] and myocardial infarction (MI) [7,8], elucidation of the effects of oxidative stress and inflammation on epidermal AF may establish basis for non-invasive evaluation of organ injury.

Keratins play multiple significant biological roles in epithelium, including intermediate filament formation [9] and inflammatory responses [10,11]. Keratins have also been used as diagnostic tumor markers [12]. Keratin 1 (K1) - keratin 10 (K10) heterodimer is a hallmarker for keratinocyte differentiation [13], which are major keratins in the suprabasal keratinocytes of epidemis[14-16]. K1 and K10 mutations are also associated with inherited skin diseases including epidermolytic ichthyosis, palmar-plantar keratoderma, and ichthyosis with confetti [17,18,19]. It is of both theoretical and clinical significance to further elucidate the biochemical and biophysical properties of keratins. While keratins is one of the four major epidermal fluorophores [4], three major questions regarding epidermal keratins' AF have remained unanswered: 1) In addition to its basal AF, can the keratins' AF be induced by pathological insults ? 2) Which keratins are responsible for the epidermal green AF under physiological and pathological conditions? 3) Does epidermal keratins' AF have any biomedical significance ?

Organ injury in numerous diseases can lead to increased levels of ROS and

inflammation in not only the organ, but also other parts of the body such as the blood circulation [5-8,20-27]. Considering that major epidermal fluorophores include the key mitochondrial electron donor NADH and a key mitochondrial electron acceptor FAD [4], it is reasonable to expect that the ROS and inflammatory factors in the blood circulation or interstitial fluid may alter epidermal AF by affecting the levels and state of these epidermal fluorophores.

Our current study determined the effects of three major types of pathological insults, including UV, oxidative stress and inflammation, on the epidermal AF in both mouse models and skin cell culture models. We also determined skin's green AF of UV-exposed human subjects, cerebral small vessel disease (CSVD) patients and AIS patients. Our study has suggested that the keratin-based epidermal green AF may become a novel biomarker for the levels of these pathological insults to the skin. These findings have also suggested that organ damage-produced inflammatory factors and ROS can produce increased epidermal green AF, which may become a common biomarker for organ injury.

Materials and Methods

Materials

All chemicals were purchased from Sigma (St. Louis, MO, USA) except where noted. Male C57BL/6SLACBL/6Slac mice, ICR mice, and BALB/cASlac-nu nude mice of SPF grade were purchased from SLRC Laboratory (Shanghai, China).

Studies on human Subjects

The study on UVC-exposures of human body was conducted according to a protocol s approved by the Ethics Committee for Human Subject Studies of Shanghai Ninth Hospital, Shanghai Jiao Tong University School of Medicine. The study on CSVD patients and AIS patients was conducted according to a protocol approved by the Ethics Committee of Shanghai Fifth People's Hospital Affiliated to Fudan University. The human subjects in our study were divided into four groups: Group 1: The group of healthy persons; Group 2: The group of CSVD patients with low-risk of developing AIS; Group 3: The group of CSVD patients with high-risk of developing AIS; and Group 4: The group of AIS patients. The age of Group 1, Group 2, Group 3 and Group 4 is 64.11±1.07, 66.80±0.65, 67.38±0.95, 64.09±1.12 years of old, respectively. The ages of all of the subjects range from 50 - 80 years of old.

Exposures of UV radiation

UVA lamp (TL-K 40W ACTINIC BL Reflector, Philips, Hamburg, Germany), UVB lamp (TL 20W/01 RS NARROWBAND, Philips, Hamburg, Germany), and UVC lamp (TUV 25W /G25 T8, Philips, Hamburg, Germany) were used as the UV sources in our experiments. C57BL/6SLACBL/6Slac mice, ICR mice, and BALB/cASlac-nu nude mice at the weight between 18-35 g were used for UVC treatment. C57BL/6SLACBL/6Slac mice at the weight between 20-30g were used for UVB or UVA treatment. After the mice were briefly anesthetized with 3.5% (w/v) chloral hydrate (1 ml /100 g), the ears of the mice were exposed to UV lamps. The power densities of UVA and UVB were 3.0±0.1 mW/cm^2 and 2.1±0.1 mW/cm^2, respectively, measured by a UVA/UVB detector (ST-513, UVAB, SENTRY

OPTRONICS CORP., Taiwan, China). The power density of UVC was 0.55±0.05 mW/cm^2, measured by a UVC detector (ST-512, UVC, SENTRY OPTRONICS CORP., Taiwan, China). The index fingers of human subjects were exposed to a UVC lamp (TUV 25W /G25 T8, Philips, Hamburg, Germany) at the power density of 2.0±0.1 mW/cm^2, with the radiation dosage of 2.4 ±0.1 J/cm^2.

Imaging of the AF of mouse's skin

The AF of the ears of the mice were imaged by a two-photon fluorescence microscope (A1 plus, Nikon Instech Co., Ltd., Tokyo, Japan), with the excitation wavelength of 488 nm and the emission wavelength of 500 - 530 nm. The AF was quantified by the following approach: Sixteen spots with the size of approximately 100 X 100 μm^2 on the scanned images were selected randomly. After the average AF intensities of each layer were calculated, the sum of the average AF intensities of all layers of each spot was calculated, which is defined as the AF intensity of each spot. If the value of average AF intensity of certain layer is below 45, the AF signal of the layer is deemed background noise, which is not counted into the sum.

The AF spectra of the mice was determined by using a two-photon fluorescence microscope (A1 plus, Nikon Instech Co., Ltd., Tokyo, Japan). After the imaging, the images were analyzed automatically. The index fingers of human subjects were imaged under a confocal fluorescence microscope (TCS SP5Ⅱ, Lecia, Wetzlar, Germany). The excitation wavelength was 488 nm and the emission wavelength was 500 - 550 nm. Eight spots with the size of approximately 200 X 200 μm^2 on the scanned images were selected randomly, which were used for calculations of the AF intensities of the fingers.

In some studies where noted, after the ears of C57BL/6SLAC mouse were irradiated with UVC, the ears were collected, which were imaged under a confocal fluorescence microscope (TCS SP5Ⅱ, Lecia, Wetzlar, Germany). The excitation wavelength was 488 nm and the emission wavelength was 500-550 nm. The AF was quantified by using the following protocol: Sixteen spots with the size of approximately 100 X 100 μm^2 on the scanned images were selected randomly. The average AF intensities of the 16 spots were quantified. The average value of the 16 AF intensities was defined as the AF intensity of the sample.

Determination of the autofluorescence of human subjects' skin and fingernails

A portable AF imaging equipment was used to detect the AF of the fingernails and certain regions of the skin of the human subjects. The excitation wavelength is 485 nm, and the emission wavelength is 500 - 550 nm. For all of the human subjects, the AF intensity in the following seven regions on both hands, i.e., fourteen regions in total, was determined, including the Index Fingernails, Ventroforefingers, Dorsal Index Finger, Centremetacarpus, Dorsal Centremetacarpus, Ventribrachium and Dorsal Antebrachium.

Determinations of the AF spectrum of human's skin

By using a portable equipment for AF spectrum determinations, we determined the spectra of the AF of the 12 regions of the skin of the human subjects. The excitation wavelength is 445 nm. The emitting light at the wavelength that is longer than 450 nm was detected.

Histology

Skin biopsies from the ears of the mice were obtained, which were placed immediately in 4% (w/v) paraformaldehyde buffer. After 12-24 hrs, paraffin embedding procedure was conducted on the samples. Hematoxylin / Eosin staining was performed according to the manufacturer's protocol (Beyotime, Haimen, Jiangsu Province, China).

Western blot assays

The lysates of the skin were centrifuged at 12,000 *g* for 20 min at 4 ℃. The protein concentrations of the samples were quantified using BCA Protein Assay Kit (Pierce Biotechonology, Rockford, IL, USA). As described previously[28], a total of 50 μg of total protein was electrophoresed through a 10% SDS-polyacrylamide gel, which were then electrotransferred to 0.45 μm nitrocellulose membranes (Millipore, CA, USA). The blots were incubated with a monoclonal Anti-Cytokeratin 1 (ab185628, Abcam, Cambridge, UK) (1:4000 dilution) or actin (1:1000, sc-58673, Santa Cruz Biotechnology, Inc., Dallas, TX, USA) with 0.05% BSA overnight at 4 ℃, then incubated with HRP conjugated Goat Anti-Rabbit IgG (H+L) (1:4000, Jackson ImmunoResearch, PA, USA) or HRP conjugated Goat Anti-mouse IgG (1:2000, HA1006, HuaBio, Zhejiang Province, China). An ECL detection system (Thermo Scientific, Pierce, IL, USA) was used to detect the protein signals. The intensities of the bands were quantified by densitometry using Image J.

Immunohistochemistry

Ten μm paraffin-sections of skin were obtained by a Leica Cryostat, mounted onto

poly-L-lysine coated slides and stored at room temperature. The skin sections were incubated in Xylene three times. The sections were then sequentially dehydrated in 100% EtOH, 95% EtOH and 70% EtOH. After two washes with PBS, the sections were blocked in 10% goat serum for 1 hr, which were then incubated in monoclonal Anti-Cytokeratin 1 (ab185628, abcam, Cambridge, UK) (1:1000 dilution), containing 1% goat serum at 4 ℃ overnight. After three washes in PBS, the sections were incubated with Alexa Fluor 647 goat anti-rabbit lgG (1:1000 dilution) (Invitrogen, CA,USA) for 1 hr in darkness at RT, followed by staining in 0.2% DAPI solution (Beyotime, Haimen, Jiangsu Province, China) for 5 min. Subsequently the sections were mounted in Fluorescence Mounting Medium (Beyotime, Haimen, Jiangsu Province, China). To compare the intensity of fluorescence in each sample, at least three randomly picked fields in each section were photographed under a Leica microscope.

Laser-based delivery of keratin 1 siRNA into mouse skin

Male C57BL/6SLACBL/6SlacMice were briefly anesthetized with 3.5% (w/v) chloral hydrate (1 ml / 100 g). After exposure to laser, the ears of the mouse were transfected with siRNA using Lipofectamine 3000 following the manufacturer's instructions (Thermo Fisher Scientific, Waltham, MA, USA). The sequences of the mouse keratin siRNA were CUCCCAUUUGGUUUGUAGCTT and UGACUGGUCACUCUUCAGCTT (GenePharma, Shanghai, China).

Statistical analyses

All data are presented as mean ± SEM. Data were assessed by one-way ANOVA,

followed by Student - Newman - Keuls *post hoc* test, except where noted. *P* values less than 0.05 were considered statistically significant.

Results

1) UV dose-dependently increased the epidermal green AF at the stratum spinosum of C57BL/6SLAC mice's ears

We determined the spectra of both the basal and the UVC-induced AF of C57BL/6SLAC mice, ICR mice and nude mice, showing that the spectra of these three strains of mice were similar, reaching maximal AF intensity at 470 - 500 nm when the excitation wavelength was 800 nm under a two-photon fluorescence microscope (**Figure 1a**). We further investigated the effects of UVC on the skin's green AF of C57BL/6SLAC mice' ears, showing that the green AF intensity of the skin was does-dependently increased by 0.33, 0.66 and 0.99 J/cm^2 UVC, assessed at 1, 6, or 24 hrs after the UVC exposures (**Figures 1b and 1c**). The green AF intensity had virtually linear relationships with the UVC dosages at 1 (r_{1h} = 0.9478), 6 (r_{6h} = 0.9448) and 24 hrs (r_{24h} = 0.9623) after the UVC exposures. Exposures of the ears' skin of ICR mice or nude mice to UVC also led to significant increases in the green AF (**Figures 1d and 1e).** Orthographic green AF images of C57BL/6SLAC mice's skin were taken to investigate the locations of the UVC-induced green AF: The UVC-induced AF increases occurred only at certain layer of the skin with the thickness of approximately 10 μm, which is approximately 10 - 20 μm apart from the outer surface of the epidermis (**Figure 1f**). Our H&E staining of the skin showed that the thickness of the epidermis is approximately 25 - 30 μm, while the thickness of the stratum corneum is less that 3 μm (**Supplemental Figure 1**), suggesting that the source of

the AF is located between the stratum corneum and the dermis. The spatial distribution of the UVC-induced AF is distinctly polyhedral (**Figures 1b and 1d**), exhibiting the characteristic structure of the suprabasal keratinocytes at the stratum spinosum of the epidermis.

We determined the effects of UVC on the green AF of B16-F10 cells - a melanoma cell line: UVC dose-dependently increased the green AF intensity of the cells (**Figures 1g – 1h**). The AF intensity had virtually linear relationships with the UVC dosages at 0.3 ($r_{0.3h}$ = 0.9478), 1 (r_{1h} = 0.9448) and 6 hrs (r_{6h} = 0.9623) after the UVC exposures. UVC also significantly increased the green AF intensity of the Ventroforefinger's skin of human subjects **(Figures 1i, 1j and 1k**).

Exposures of the ears of C57BL/6SLAC mice to 1.3 and 2.6 J/cm^2 UVB also led to dose-dependent increases in the green AF, assessed at 6 and 24 hrs after the exposures (**Supplemental Figures 2a and 2b**). The AF intensity had virtually linear relationships with the UVB dosage at 6 (r_{6h} = 0.9997) and 24 hr (r_{24h} = 0.9742) after the UVB exposures. Exposures of the ears of C57BL/6SLAC mice to UVA at the dosage of 5.4 J/cm^2 led to a significant AF increase at 24 hrs after the exposures (**Supplemental Figures 2c and 2d**). The AF intensity also had virtually linear relationships with the UVA dosages at 6 (r_{6h} = 0.9741) and 24 hr (r_{24h} = 0.9361) after the UVA exposures. The spectra of UVC-, UVB-, and UVA-induced AF were similar, reaching its peak at 470 - 480 nm when the excitation wavelength was 800 nm under a two-photon microscope (**Supplemental Figure 2e)**.

2) Evidence suggesting that keratin 1 is the major source of the UV-induced epidermal green AF of C57BL/6SLAC mice's ear

The spectrum of the UV-induced green AF is distinctly different from that of NADH [29,30], thus excluding the possibility that NADH is responsible for the UV-induced green AF. Our observation that the UVC-induced green AF mainly occurs in the stratum spinosum argues against the possibility that FAD is responsible for the UV-induced AF increases, considering that FAD is an ubiquitous molecule. Moreover, UVC produced a significant decrease in the FAD level of the skin of C57BL/6SLAC's ears at 1 hr after the UVC exposures (**Supplemental Figure 3**), when UVC significantly increased the AF intensity (**Figures 2b and 2c**), arguing further against the possibility that FAD is responsible for the UVC-induced AF increase. Because UVC can induce significant increases in the AF of the skin of ICR mice's ears (**Figure 1e)**, a strain of albino mice that are melanin-deficient [31], it is unlikely that melanin is responsible for the UVC-induced increase in the AF. Moreover, our observation that Deoxyadenosine (DA), a competitive melanin synthesis inhibitor, did not affect the UVC-induced increase in the green AF of B16-F10 cells (data not shown) further excludes the possibility that melanin is responsible for the increased AF. Collectively, the discussion above has implicated that epidermal keratins may be responsible for the UV-induced epidermal green AF, since melanin, FAD, NADH and keratins are four major known epidermal fluorophores[4].

Several lines of evidence has suggested that K1 and K10 may be the two major potential sources of the UV-induced epidermal green AF: First, the spectrum of the UV-induced green AF (**Figure 1a**) matches that of the keratins' AF [32]. Second, the spatial distribution of the UV-induced AF exhibits the characteristic structure of the suprabasal keratinocytes at the stratum spinosum (**Figures 1b and 1d**), in which K1 and K10 are the major keratins [14,15,16]. Third, K1-K10 heterodimers, the major existing form of K1 and K10 in the suprabasal

keratinocytes, form the unique, highly dense bundles that are parallel with the cell membranes of the suprabasal cells [33 34]. Our TEM study on the ear's epidermis of C57BL/6SLAC mice has also found polyhedral structures and dense bundles in the layers between the stratum corneum and the dermis (**Supplemental Figure 4**). Moreover, immunostaining of the skin of C57BL/6SLAC mice's ears using anti-K1 antibody also showed polyhedral structure of the K1-positive regions (**Supplemental Figure 5**). This unique spatial distribution of the K1-K10 heterodimers matches well with the spatial distribution of the UVC-induced green AF (**Figures 1b and 1d**).

We determined the levels of K1 and K10 in the ear's skin of C57BL/6SLAC mice and nude mice, and in B16-F10 cells and HaCaT cells - two widely used skin cell lines. In the ears of C57BL/6SLAC mouse and nude mouse, K10 existed mainly in the 60 kDa form and 54 kDa form, respectively (**Figures 2a and 2b**), while there was only a very low level of K10 in HaCaT cells (**Figures 2a and 2b**). There was a 67 kDa band of K1 in HaCaT cells (**Figures 2a and 2b**). In contrast, under the normal denaturing conditions for Western Blot analyses on the samples prepared from the C57BL/6SLAC mouse's ears, nude mouse's ears and B16-F10 cells, the K1 antibody recognized two bands at 127 kDa and 67 kDa, respectively, with the 127 kDa band as the predominant band (**Figures 2a and 2b**). Two lines of evidence has suggested that the K1-containing band of 127 kDa is the K1-K10 heterodimer: First, it is established that K1 and K10 form heterodimers through covalent binding in the stratum spinosum [35], which may be dissociated when urea concentration is in molar range [33]; and second, the sum of the molecular weight of K1 and K10 is approximately 127 kDa.

We determined the K1 and K10 levels of the ears and back of both C57BL/6SLAC mice

and nude mice: The level of the K1-K10 heterodimers in the skin of C57BL/6SLAC mice's back was only approximately 6% of that of C57BL/6SLAC mice's ears, while the levels of the K1-K10 heterodimers in both the ears and back of nude mice's are significantly higher than those in C57BL/6SLAC mice's ears and back (**Figures 2c and 2d**). There was the K10 of both 60 kDa and 54 kDa in the ears and back of nude mice, while there was only the K10 of 60 kDa in both the ear and the back of C57BL/6SLAC mice (**Figures 2c and 2d**).

We determined both the basal and UVC-induced epidermal green AF of C57BL/6SLAC mice's ears and back: While UVC induced a significant increase in the green AF of C57BL/6SLAC mice's ears, UVC did not significantly affect the green AF of C57BL/6SLAC mice's back (**Figures 2e and 2f**). In contrast, UVC induced significant increases in the green AF of both the ears and the back of nude mice (**Figures 2e and 2f**). There was no significant difference among the FAD levels in the ears and the back of C57BL/6SLAC mice and nude mice (**Supplemental Figure 6**). Together with the above-stated evidence suggesting that K1 and K10 are two major potential sources of the UVC-induced epidermal green AF, our observation that the presence of K10 with virtual absence of K1 is associated with the absence of the UVC-induced epidermal green AF in C57BL/6SLAC mouse's back has suggested that K1, but not K10, is the major source of the UVC-induced epidermal green AF.

We further applied laser-based technology to deliver K1 siRNA into the skin of C57BL/6SLAC mice's ears to determine the role of K1 in the UVC-induced AF. The laser treatment led to marked increases in the fluorescent signal of Cy5-labeled siRNA inside the skin (**Supplemental Figure 7**), suggesting the effectiveness of the siRNA delivery. Our Western blot assays showed that the laser-based K1 siRNA administration led to a significant decrease in

the K1 levels of the ears (**Figures 2g and 2h**). Immunostaining of the skin showed similar results (**Figure 2i**). The K1 siRNA administration led to a significant reduction of the UVC-induced AF intensity (**Figures 2j and 2k**).

3) UVC-generated ROS produces K1 degradation that can lead to increased epidermal green AF and cell death

Our study showed that UVC induced a significant decrease in the K1 of 127 kDa 30 min after the ears of C57BL/6SLAC mice were exposed to 0.33 J/cm^2 or 0.66 J/cm^2 UVC (**Figures 3a and 3b**). UVC also produced a significant decrease in the K1 levels of B 16 cells (**Figures 3c and 3d**). These findings have suggested that K1 degradation, instead of K1 increase, is associated with the UVC-induced AF increase. E-64, a broad spectrum cysteine protease inhibitor, significantly attenuated the UVC-induced increase in the epidermal green AF of C57BL/6SLAC mice's ear (**Figures 3e and 3f**), suggesting that UVC induces increased epidermal green AF by producing K1 degradation. E-64 administration also prevented UVC-induced K1 degradation (**Supplemental Figures 8a and 8b**).

Our AF imaging study showed that topical administration of 3 or 7.5 mg/cm^2 N-acetyl cysteine (NAC), an antioxidant, led to a significant decrease in the 0.66 J/cm^2 UVC-induced epidermal AF of the C57BL/6SLAC mice's ears 1 hr after the UVC exposures (**Figures 3g and 3h**). The UVC-induced K1 degradation was also prevented by the NAC administration (**Figures 3i and 3j**).

In the skin cell lines that have K1 monomers only, UVC also induced increased green AF: There was a selective increase in the K1 monomers in the B16-F10 cells overexpressing K1

with Flag at its C-terminus (**Supplemental Figure 9a**), in which a marked increase in green AF was induced by UVC (**Supplemental Figure 9b**). UVC also produced a marked decrease in the levels of K1 monomers of the cells overexpressing the Flagged-K1 (**Supplemental Figure 9a)**.

We further determined the effects of decreased K1 levels on B16-F10 cell survival, showing that K1 siRNA, but not K10 siRNA, dose-dependently induced early-stage (Annexin V^+/AAD^-) and late-stage apoptosis (Annexin V^+/AAD^+) as well as necrosis (Annexin V^-/AAD^+) of the cells (**Figures 3k – 3l**). K1 siRNA, but not K10 siRNA, also induced increases in the fluorescence intensity of both dichlorofluorescein (DCF) (**Figure 3m**) and ethidium (**Figure 3n**) of the cells - two fluorescent markers of ROS, suggesting that decreased K1 may induce the cell death at least partially by exacerbating oxidative stress.

4) LPS and oxidative stress can induce increased green AF of the skin of C57BL/6SLAC mice' ears or B16-F10 cells, respectively

The skin's green AF of C57BL/6SLAC mice's ears was determined at 1 hr, 1 day, 3 day and 7 day after the mice were administered with 1 mg/kg LPS by i.p. injection. LPS induced significant increases in the green AF at all of these time points (**Figures 4a and 4b**). We also determined the effects of 0.1, 0.5 and 1 mg/kg LPS on the green AF, showing that LPS dose-dependently induced increases in the green AF, assessed at both 3 (**Figures 4c and 4d**) and 7 days (**Figures 4e and 4f**) after the LPS administration. The AF intensity had linear relationships with the LPS dosages at both 3 days (R^2 = 0.9697) and 7 days (R^2 = 0.9889) after the LPS administration. These AF images exhibited the characteristic polyhedral

structure of the keratinocytes in stratum spinosum. We also found that H_2O_2 concentration-dependently increased the green AF intensity of B16-F10 cells (**Figures 4g – 4h**). The AF intensity also had linear relationships with the H_2O_2 concentrations at both 0.3 mM H_2O_2 (R^2 = 0.9897) and 0.5 mM H_2O_2 (R^2 = 0.9739).

5) The green AF intensity of skin is highly correlated with the risk of CSVD patients to develop AIS

We further determined the green AF intensity of the skin of healthy controls, the CSVD patients at either low-risk or high-risk to develop AIS, and AIS patients. In the Dorsal Index Fingers of certain AIS patients, there were characteristic green AF structures that were similar with those observed in the UVC-exposed ears' skin of C57BL/6SLAC mice (data not shown), suggesting that at least for Dorsal Index Fingers of AIS patients, the green AF also existed in the stratum spinosum of human's epidermis. The epidermal green AF intensity at both right (R^2 = 0.9997) and left Dorsal Index Fingers (R^2 = 0.9884) was highly correlated with the risk level of the CSVD patients to develop AIS (**Figures 5a and 5b**). The epidermal green AF intensity at both right (R^2 = 0.9530) and left Ventroforefinger (R^2 = 0.9979) was also highly correlated with the risk level of the CSVD patients to develop AIS (**Figures 5a and 5b**).

There was marked variability in the basal AF intensity of the various regions of the skin of healthy people (**Figures 5c and 5d**), the CSVD patients (**Figures 5e and 5f**) and the AIS patients (**Figures 5g and 5h**). The variability did not appear to be associated with sunshine exposures, since the AF intensity of the Ventroforefinger was significantly higher than that of Dorsal Index Fingers on either left side or right side in all of these groups. Compared with the

healthy group, the extent of the variability of the AIS group was markedly higher: The difference between the AF intensity of Ventroforefinger and Ventriantebrachium on the right and left side of AIS patients was approximately 150% and 70%, respectively, while the difference between the AF intensity of Ventroforefinger and Ventriantebrachium on the right and left side of healthy people was approximately 20% and 40%, respectively.

Discussion

Since inflammation and oxidative stress are two common key pathological factors in organ injury, it is of critical significance to search for biomarkers for non-invasive evaluation of the levels of inflammation and oxidative stress in the body. Since epidermal AF may be affected by the ROS and inflammatory factors that are transported through such pathways as the blood circulation, changes of epidermal AF may become the first biomarker of the ROS and inflammatory factors in the body. Our current study has suggested that epidermal green AF may become the first endogenous indicator of the levels of ROS and inflammatory factors to which the skin is exposed: First, epidermal green AF intensity has virtually linear relationships with the dosages of UV and LPS in mouse model studies; green AF intensity has virtually linear relationships with dosages of ROS in skin cell cultures; and the green AF intensity of human's skin is also highly correlated with the risk of CSVD patients to develop AIS. For healthy skin, the ROS and inflammatory factors to which the skin is exposed should come from such pathways as the blood circulation. Therefore, epidermal green AF may also become the first biomarker of the levels of oxidative stress and inflammation in the body.

Our study has also suggested that increased epidermal green AF is a strong indicator of

‘real damage levels’ of cells and tissues: First, our study has indicated that K1 degradation mediates the UV-induced increases in the green AF intensity. The findings indicating critical biological functions of K1 and the observation showing perinatal lethality of K1-knockout mice [10] have suggested that K1 degradation may lead to tissue and cellular damage. Indeed, our study has indicated that decreased K1 levels can lead to both apoptosis and necrosis of a skin cell line. Second, our findings showing virtually linear relationships between the intensity of UV-, LPS- and ROS-induced green AF and the dosages of these pathological insults have also suggested that the epidermal green AF is an indicator of ‘real damage levels’ of cells and tissues, since it is established that these pathological insults can dose-dependently produce cellular and tissue damage.

Our previous studies have indicated that the patients of each of the five diseases we have studied, including AIS [36], MI [37], stable coronary artery disease [37], Parkinson’s disease [38] and lung cancer [39] patients have their characteristic patterns of green AF in multiple skin locations, which was defined as ‘Pattern of AF’. ‘Pattern of AF’ is formed by several major properties of the green AF of the skin, including AF intensity, AF asymmetry, locations with the AF changes and structure of the green AF images. By generalizing the properties of the skin’s green AF of the patients of each disease, as we have studied on the five major diseases[36,37,38,39], we may establish the unique ‘Pattern of AF’ of each disease, which may be used to provide non-invasive diagnosis of the diseases.

However, the mechanisms underlying the ‘Pattern of AF’-based diagnostic approach have remained unclear. Our current study has provided critical information for elucidating the mechanisms: Our study has indicated that both inflammation and oxidative stress can induce

increased epidermal green AF. Significant increases in the levels of oxidative stress and inflammatory factors have been found in the patients' body of CVSD [40,41], AIS [20-22], MI [23-27], lung cancer [42-46], Parkinsons' disease [47-49], stable coronary artery diseases [26,50-53], hypertension [54,55] and diabetes [56-58]. Therefore, we proposed that the increased green AF in the patients' skin of the diseases may result from the elevated oxidative stress and inflammation in their body. Blood circulation is the leading pathway by which ROS and inflammatory factors may be transported along the body. However, our findings regarding the remarkable variability of the AF increases in the skin of the AIS and CSVD patients have argued against the possibility that the blood circulation is the pathway by which ROS and inflammatory factors are transmitted to the locations of the skin: If were the AF increases produced by the ROS and inflammatory factors in the blood circulation, the green AF intensity in the various locations of the human skin would be relatively homogeneous.

We have proposed the hypothesis that ROS and inflammatory factors might be transported along the Meridian System ('Channel System'), the pivotal system in Chinese medicine, that links the locations of the skin to the damaged organ [36]: The damaged organ in a certain disease could produce significant levels of oxidative stress and inflammation, which may be transported along the Meridian System that corresponds to the organ, leading to 'Blockage' ('Yu Du' in Chinese) of the system. The ROS and inflammatory factors that are transported along the channel may diffuse into the suprabasal layer of the epidermis, leading to keratin degradation and subsequent increases in the epidermal green AF. Therefore, different injury levels of a certain organ may lead to differential changes of the green AF at various locations of the skin along the Meridian System that corresponds to the organ, forming its

characteristic 'Pattern of AF'. We have obtained significant evidence supporting this hypothesis, e.g., there were marked and selective increases in the skin's green AF at certain locations for both lung cancer patients[39] and professional swimmers [59]. However, extensive future studies are required to further test the validity of this hypothesis. If this hypothesis is demonstrated, our understanding on the scientific basis of Chinese medicine would be profoundly enhanced. This demonstration would also provide an essential linkage between Western medicine and Chinese medicine.

Based on these pieces of information, we have proposed our novel theory for non-invasive evaluation of organ injury - 'Pattern of AF Theory for Organ Injury' (**Figure 6**): Injury of a certain organ can release major pathological factors such as ROS and inflammatory factors, which may be transported along the Meridian System that links to the organ. The ROS and inflammatory factors can induce keratin degradation of the epidermis nearby the Meridian System, leading to increased green AF intensity at those locations of the skin. Therefore, each different injury level of a certain organ can lead to differential changes of green AF at various locations of the skin along the Meridian System, forming its characteristic 'Pattern of AF'. By determining the 'Pattern of AF', we can evaluate non-invasively the injury level of a certain organ.

Our green AF-based method for evaluating pathological state is essentially a 'organ damage-detection method', which can provide not only non-invasive diagnosis of numerous diseases, but also non-invasive evaluation of sub-health conditions as well as therapeutic effects on numerous diseases. Our 'organ damage-detection method' has also surpassed previous methods of 'risk evaluation'. For example, since our AF-based approach may determine the

injury levels of cardiovascular and cerebrovascular system, our approach may have profoundly higher precision in evaluating the risk of a person to develop AIS or MI than previously used methods.

Our study has also exposed several novel biological and pathological properties of keratins: First, our finding showing that UVC can induce K1 degradation by such mechanisms as increasing oxidative stress and cysteine protease activity, together with our finding showing the capacity of decreased K1 to induce oxidative stress as well as apoptosis and necrosis of cells, have suggested a novel mechanism underlying UV-induced skin damage - the 'Keratin Degradation-Mediated Skin Damage Theory for UV-Induced Skin Damage' (**Figure 7**). These findings may also shed light for elucidating the pathological mechanisms underlying the K1 mutations-associated inherited skin diseases. Second, our study has indicated novel properties of epidermal keratins' AF: In addition to its basal AF, epidermal keratins' AF can also be induced by such pathological insults as UV, inflammation and ROS, in which K1 is a key factor. Most previous studies regarding AF applications in disease diagnosis have determined basal AF only. Our study has suggested that determinations of both basal AF and 'induced AF' may provide significantly richer information for the biomedical applications of epidermal keratins' AF. Third, epidermal keratins' AF have extensive biological significance: It is not only a biomarker for indicating the pathological damage of skin, but also a novel, common biomarker for organ damage. Moreover, since it is established that UV exposures at a certain time point can dose-dependently produce skin damage in the future, our finding that the dosages of UV have virtually linear relationships with the epidermal green AF intensity has suggested that the AF intensity may also become the first biomarker for predicating UV-induced skin damage.

Furthermore, our study has suggested profound variability of the biological properties of keratins in different parts of mice's body and different strains of mice, which have highlighted the complexity of both epidermal keratins and the skin.

A**cknowledgment:**

The authors would like to acknowledge the financial support by a Major Research Grant from the Scientific Committee of Shanghai Municipality #16JC1400500 and #16JC1400502 (to W.Y.), and a Major Special Program Grant of Shanghai Municipality (Grant # 2017SHZDZX01) (to W.Y.). The authors acknowledges highly valuable discussion with Prof. Jianpeng Ma, Prof. Jiucun Wang, Prof. Xingdong Chen from Fudan University, and Prof. Yu Wang from Shanghai University of Chinese Medicine.

References:

1 Moran, C. *et al.* Type 2 diabetes, skin autofluorescence, and brain atrophy. *Diabetes* **64**, 279-283, doi:10.2337/db14-0506 (2015).

2 Takeuchi, Y. *et al.* Autofluorescence imaging of early colorectal cancer. *Journal of biophotonics* **4**, 490-497, doi:10.1002/jbio.201100013 (2011).

3 Pena, A., Strupler, M., Boulesteix, T. & Schanne-Klein, M. Spectroscopic analysis of keratin endogenous signal for skin multiphoton microscopy. *Optics express* **13**, 6268-6274 (2005).

4 Bader, A. N. *et al.* Fast nonlinear spectral microscopy of in vivo human skin. *Biomedical optics express* **2**, 365-373, doi:10.1364/BOE.2.000365 (2011).

5 Chen, H. *et al.* Oxidative stress in ischemic brain damage: mechanisms of cell death and potential molecular targets for neuroprotection. *Antioxid Redox Signal* **14**, 1505-1517, doi:10.1089/ars.2010.3576 (2011).

6 Wimmer, I., Zrzavy, T. & Lassmann, H. Neuroinflammatory responses in experimental and human stroke lesions. *Journal of neuroimmunology* **323**, 10-18, doi:10.1016/j.jneuroim.2018.07.003 (2018).

7 Sinning, C., Westermann, D. & Clemmensen, P. Oxidative stress in ischemia and reperfusion: current concepts, novel ideas and future perspectives. *Biomark Med* **11**, 11031-11040, doi:10.2217/bmm-2017-0110 (2017).

8 Kain, V., Prabhu, S. D. & Halade, G. V. Inflammation revisited: inflammation versus resolution of inflammation following myocardial infarction. *Basic Res Cardiol* **109**, 444, doi:10.1007/s00395-014-0444-7 (2014).

9 Schweizer, J. *et al.* New consensus nomenclature for mammalian keratins. *The Journal of cell biology* **174**, 169-174, doi:10.1083/jcb.200603161 (2006).

10 Roth, W. *et al.* Keratin 1 maintains skin integrity and participates in an inflammatory network in skin through interleukin-18. *Journal of cell science* **125**, 5269-5279, doi:10.1242/jcs.116574 (2012).

11 Hobbs, R. P., Lessard, J. C. & Coulombe, P. A. Keratin intermediate filament proteins - novel regulators of inflammation and immunity in skin. *Journal of cell science* **125**, 5257-5258, doi:10.1242/jcs.122929 (2012).

12 Karantza, V. Keratins in health and cancer: more than mere epithelial cell markers. *Oncogene* **30**, 127-138, doi:10.1038/onc.2010.456 (2011).

13 Woodcock-Mitchell, J., Eichner, R., Nelson, W. G. & Sun, T. T. Immunolocalization of keratin polypeptides in human epidermis using monoclonal antibodies. *The Journal of cell biology* **95**, 580-588 (1982).

14 Moll, R., Franke, W. W., Schiller, D. L., Geiger, B. & Krepler, R. The catalog of human cytokeratins: patterns of expression in normal epithelia, tumors and cultured cells. *Cell* **31**, 11-24 (1982).

15 Eichner, R., Bonitz, P. & Sun, T. T. Classification of epidermal keratins according to their immunoreactivity, isoelectric point, and mode of expression. *The Journal of cell biology* **98**, 1388-1396 (1984).

16 Sun, T. T. *et al.* Keratin classes: molecular markers for different types of epithelial differentiation. *The Journal of investigative dermatology* **81**, 109s-115s (1983).

17 Lacz, N. L., Schwartz, R. A. & Kihiczak, G. Epidermolytic hyperkeratosis: a keratin

1 or 10 mutational event. *Int J Dermatol* **44**, 1-6, doi:10.1111/j.1365-4632.2004.02364.x (2005).

18 Smith, F. J. D. *et al.* Novel and recurrent mutations in keratin 1 cause epidermolytic ichthyosis and palmoplantar keratoderma. *Clin Exp Dermatol*, doi:10.1111/ced.13800 (2018).

19 Toivola, D. M., Boor, P., Alam, C. & Strnad, P. Keratins in health and disease. *Current opinion in cell biology* **32**, 73-81, doi:10.1016/j.ceb.2014.12.008 (2015).

20 Seet, R. C. *et al.* Oxidative damage in ischemic stroke revealed using multiple biomarkers. *Stroke* **42**, 2326-2329, doi:10.1161/STROKEAHA.111.618835 (2011).

21 Ciancarelli, I., Di Massimo, C., De Amicis, D., Carolei, A. & Tozzi Ciancarelli, M. G. Evidence of redox unbalance in post-acute ischemic stroke patients. *Curr Neurovasc Res* **9**, 85-90 (2012).

22 Dominguez, C. *et al.* Oxidative stress after thrombolysis-induced reperfusion in human stroke. *Stroke* **41**, 653-660, doi:10.1161/STROKEAHA.109.571935 (2010).

23 Mocatta, T. J. *et al.* Plasma concentrations of myeloperoxidase predict mortality after myocardial infarction. *J Am Coll Cardiol* **49**, 1993-2000, doi:10.1016/j.jacc.2007.02.040 (2007).

24 Deepa, M., Pasupathi, P., Sankar, K. B., Rani, P. & Kumar, S. P. Free radicals and antioxidant status in acute myocardial infarction patients with and without diabetes mellitus. *Bangladesh Med Res Counc Bull* **35**, 95-100 (2009).

25 Caimi, G. *et al.* Behaviour of protein carbonyl groups in juvenile myocardial infarction. *Clin Hemorheol Microcirc* **53**, 297-302, doi:10.3233/CH-2012-1551

(2013).

26 Uppal, N., Uppal, V. & Uppal, P. Progression of Coronary Artery Disease (CAD) from Stable Angina (SA) Towards Myocardial Infarction (MI): Role of Oxidative Stress. *J Clin Diagn Res* **8**, 40-43, doi:10.7860/JCDR/2014/7966.4002 (2014).

27 Madole, M. B., Bachewar, N. P. & Aiyar, C. M. Study of oxidants and antioxidants in patients of acute myocardial infarction. *Adv Biomed Res* **4**, 241, doi:10.4103/2277-9175.168608 (2015).

28 Sheng, C. *et al.* NAD^+ administration significantly attenuates synchrotron radiation X-ray-induced DNA damage and structural alterations of rodent testes. *International journal of physiology, pathophysiology and pharmacology* **4**, 1-9 (2012).

29 Islam, M. S., Honma, M., Nakabayashi, T., Kinjo, M. & Ohta, N. pH dependence of the fluorescence lifetime of FAD in solution and in cells. *International journal of molecular sciences* **14**, 1952-1963, doi:10.3390/ijms14011952 (2013).

30 Huang, Z. *et al.* Cutaneous melanin exhibiting fluorescence emission under near-infrared light excitation. *Journal of biomedical optics* **11**, 34010, doi:10.1117/1.2204007 (2006).

31 Beermann, F. *et al.* Rescue of the albino phenotype by introduction of a functional tyrosinase gene into mice. *The EMBO journal* **9**, 2819-2826 (1990).

32 Zvyagin, A. V. *et al.* Imaging of zinc oxide nanoparticle penetration in human skin in vitro and in vivo. *Journal of biomedical optics* **13**, 064031, doi:10.1117/1.3041492 (2008).

33 Reichelt, J., Bussow, H., Grund, C. & Magin, T. M. Formation of a normal epidermis

supported by increased stability of keratins 5 and 14 in keratin 10 null mice. *Molecular biology of the cell* **12**, 1557-1568, doi:10.1091/mbc.12.6.1557 (2001).

34 P A Coulombe, K. M. B., and C-H Lee. Keratins and the Skin. *Cell Architecture and Function.*, 665-671. (2013.).

35 Thiele, J. J., Hsieh, S. N., Briviba, K. & Sies, H. Protein oxidation in human stratum corneum: susceptibility of keratins to oxidation in vitro and presence of a keratin oxidation gradient in vivo. *J Invest Dermatol* **113**, 335-339, doi:10.1046/j.1523-1747.1999.00693.x (1999).

36 Wu D., Zhang M., Tao Y., Li Y., Zhang S., Chen X., Ying W. Distinct pattern of autofluorescence of the skin and fingernails of acute ischemic stroke patients: A novel diagnostic biomarker for acute ischemic stroke. *bioRxiv*, 310904, doi:https://doi.org/10.1101/310904 (2018).

37 Qu X., Li Y., Tao Y., Zhang M., Wu D., Guan S., Han W., Ying W. Distinct patterns of the autofluorescence of body surface: Potential novel diagnostic biomarkers for stable coronary artery disease and myocardial infarction. *bioRxiv* 330985, doi:https://doi.org/10.1101/330985 (2018).

38 Wu D., Tao Y., Zhang M., Li Y., Shen L., Li Y., Ying W. Selectively increased autofluorescence at fingernails and certain regions of skin: A potential novel diagnostic biomarker for Parkinson disease. *bioRxiv 322222*, doi:https://doi.org/10.1101/322222 (2018).

39 Zhang M., Tao Y., Chang Q., Li Y., Chu T., Ying W. Selectively increased autofluorescence at certain regions of skin may become a novel diagnostic biomarker

for lung cancer. *bioRxiv* 315440, doi:https://doi.org/10.1101/315440 (2018).

40 Grochowski, C., Litak, J., Kamieniak, P. & Maciejewski, R. Oxidative stress in cerebral small vessel disease. Role of reactive species. *Free Radic Res* **52**, 1-13, doi:10.1080/10715762.2017.1402304 (2018).

41 Staszewski, J., Piusinska-Macoch, R., Brodacki, B., Skrobowska, E. & Stepien, A. IL-6, PF-4, sCD40 L, and homocysteine are associated with the radiological progression of cerebral small-vessel disease: a 2-year follow-up study. *Clin Interv Aging* **13**, 1135-1141, doi:10.2147/CIA.S166773 (2018).

42 de Cavanagh, E. M. *et al.* Higher oxidation and lower antioxidant levels in peripheral blood plasma and bone marrow plasma from advanced cancer patients. *Cancer* **94**, 3247-3251, doi:10.1002/cncr.10611 (2002).

43 Tsao, S. M., Yin, M. C. & Liu, W. H. Oxidant stress and B vitamins status in patients with non-small cell lung cancer. *Nutr Cancer* **59**, 8-13, doi:10.1080/01635580701365043 (2007).

44 Margaret, A. L., Syahruddin, E. & Wanandi, S. I. Low activity of manganese superoxide dismutase (MnSOD) in blood of lung cancer patients with smoking history: relationship to oxidative stress. *Asian Pac J Cancer Prev* **12**, 3049-3053 (2011).

45 Look, M. P. & Musch, E. Lipid peroxides in the polychemotherapy of cancer patients. *Chemotherapy* **40**, 8-15, doi:10.1159/000239163 (1994).

46 Peddireddy, V., Siva Prasad, B., Gundimeda, S. D., Penagaluru, P. R. & Mundluru, H. P. Assessment of 8-oxo-7, 8-dihydro-2'-deoxyguanosine and malondialdehyde levels

as oxidative stress markers and antioxidant status in non-small cell lung cancer. *Biomarkers* **17**, 261-268, doi:10.3109/1354750X.2012.664169 (2012).

47 de Farias, C. C. *et al.* Highly specific changes in antioxidant levels and lipid peroxidation in Parkinson's disease and its progression: Disease and staging biomarkers and new drug targets. *Neurosci Lett* **617**, 66-71, doi:10.1016/j.neulet.2016.02.011 (2016).

48 Duran, R. *et al.* Oxidative stress and aminopeptidases in Parkinson's disease patients with and without treatment. *Neurodegener Dis* **8**, 109-116, doi:10.1159/000315404 (2011).

49 Andican, G. *et al.* Plasma oxidative and inflammatory markers in patients with idiopathic Parkinson's disease. *Acta Neurol Belg* **112**, 155-159, doi:10.1007/s13760-012-0015-3 (2012).

50 Baseri, M. *et al.* Myeloperoxidase levels predicts angiographic severity of coronary artery disease in patients with chronic stable angina. *Adv Biomed Res* **3**, 139, doi:10.4103/2277-9175.135155 (2014).

51 Bilinska, M. *et al.* Antioxidative activity of sulodexide, a glycosaminoglycan, in patients with stable coronary artery disease: a pilot study. *Med Sci Monit* **15**, CR618-623 (2009).

52 Kamezaki, F. *et al.* Serum soluble lectin-like oxidized low-density lipoprotein receptor-1 correlates with oxidative stress markers in stable coronary artery disease. *Int J Cardiol* **134**, 285-287, doi:10.1016/j.ijcard.2007.12.069 (2009).

53 Kiliszek, M. *et al.* Low-density lipoprotein reduction by sirrivastatin is accompanied

by angiotensin II type 1 receptor downregulation, reduced oxidative stress, and improved endothelial function in patients with stable coronary artery disease. *Coronary Artery Dis* **18**, 201-209, doi:DOI 10.1097/MCA.0b013e32802c7cb0 (2007).

54 Houston, M. C. Nutrition and nutraceutical supplements in the treatment of hypertension. *Expert Rev Cardiovasc Ther* **8**, 821-833, doi:10.1586/erc.10.63 (2010).

55 Montezano, A. C. *et al.* Oxidative stress and human hypertension: vascular mechanisms, biomarkers, and novel therapies. *Can J Cardiol* **31**, 631-641, doi:10.1016/j.cjca.2015.02.008 (2015).

56 Rosen, P. *et al.* The role of oxidative stress in the onset and progression of diabetes and its complications: a summary of a Congress Series sponsored by UNESCO-MCBN, the American Diabetes Association and the German Diabetes Society. *Diabetes Metab Res Rev* **17**, 189-212 (2001).

57 Samadi, A. *et al.* Oxysterol species: reliable markers of oxidative stress in diabetes mellitus. *J Endocrinol Invest*, doi:10.1007/s40618-018-0873-5 (2018).

58 Evans, J. L., Goldfine, I. D., Maddux, B. A. & Grodsky, G. M. Oxidative stress and stress-activated signaling pathways: a unifying hypothesis of type 2 diabetes. *Endocr Rev* **23**, 599-622, doi:10.1210/er.2001-0039 (2002).

59 Tao Y., Zhang M., Li Y., Shen X., Ying W. Professional swimmers and normal populations have different patterns of epidermal green autofluorescence. *bioRxiv*, 510891.

Figure Legends:

Figure 1. UV dose-dependently increased the epidermal green AF at the stratum spinosum of C57BL/6SLAC mice's ears. (a) The spectra of the epidermal AF of the UVC-induced AF of C57BL/6SLAC, ICR and nude mice were determined, showing that the spectra of the three strains of mice were similar. N = 3 for each strain of the mice. The data are the representative of the epidermal AF's spectrum of one mice for each strain. (b) Exposures of the skin to 0.33, 0.66 or 0.99 J/cm^2 UVC led to dose-dependent increases in the skin's AF of C57BL/6SLAC mice's ears, assessed at 0, 1, 6 or 24 hrs after the UVC exposures. Excitation wavelength = 488 nm and emission wavelength = 500 - 530 nm. Scale bar = 20 μm. (c) Quantifications of the AF showed that each dose of UVC induced a significant increase in the epidermal AF of C57BL/6SLAC mice's ears. *, $P < 0.05$; ***, $P < 0.001$. N = 10 – 13. (d) Exposures of the skin of the ears of C57BL/6SLAC, ICR and nude mice to UVC led to increases in the green AF. The AF was assessed at 3 - 6 hrs after the UVC exposures. Scale bar = 20 μm. (e) Quantifications of the AF showed that UVC induced significant increases in the skin's AF of the ears of C57BL/6SLAC, ICR and nude mice. **, $P < 0.01$; ***, $P < 0.001$. N = 4 – 5. (f) The distribution of the AF exhibited the characteristic structure of the keratinocytes at stratum spinosum. The AF was originated from the layer of the epidermis which is approximately 10 - 20 μm from the outer layer of the stratum corneum. The images of XY axis (square), YZ axis (76 μm in length, left column) and XZ axis (76 μm in length, bottom column) were shown. (g) Exposures of the Vetroforefinger's skin of human subjects to 2.4 J/cm^2 UVC led to increased green AF of the skin, assessed immediately after the UVC exposures. Excitation wavelength = 488 nm and

emission wavelength = 500 - 530 nm. Scale bar = 100 μm. (h) The bar graph shows the AF intensity of each subject before or after the UVC exposures. (i) Quantifications of the AF showed that UVC induced a significant increase in the AF of human skin. ***, $P < 0.001$. N = 12.

Figure 2. Evidence suggesting that keratin 1 is the major source of the UV-induced epidermal green AF of C57BL/6SLAC mice's ear. (a, b) Western blot assays of the K1 and K10 in the ears of B16-F10 cell, HaCaT cells, C57BL/6SLAC mice and nude mice. *, $P < 0.05$; **, $P < 0.01$; ***, $P < 0.001$. N = 12. (c, d) Western blot assays of the K1 and K10 in the ears and the back of C57BL/6SLAC mice and nude mice. **, $P < 0.01$; ***, $P < 0.001$. N = 6. (e, f) The basal and UVC-induced epidermal green AF of the ears and back of C57BL/6SLAC mice and nude mice. *, $P < 0.05$; **, $P < 0.01$; ***, $P < 0.001$. N = 12-15. (g) Western blot assays showed that the laser-based keratin 1 siRNA administration led to decreased keratin 1 levels in the ears of C57BL/6SLAC mice. (h) Quantifications of the Western blot showed that the laser-based keratin 1 siRNA administration led to a significant decrease in the keratin 1 levels in the ears. *, $P < 0.05$; **, $P < 0.01$. N = 6 - 7. (i) Immunostaining of the skin showed that the laser-based keratin 1 siRNA administration led to an obvious decrease in the keratin 1 levels in the epidermis. (j) The keratin 1 siRNA administration led to decreases in the UVC-induced epidermal AF of the ears of C57BL/6SLAC mice. (k) Quantifications of the AF indicated that the laser-based keratin 1 siRNA administration led to a significant decrease in the UVC-induced AF. ***, $P < 0.001$. N = 6 - 10.

Figure 3. UVC-generated ROS produces K1 degradation that can lead to both increased epidermal green AF and cell death. (a) Western blot assays showed that exposures of 0.33 or 0.66 J/cm^2 UVC dose-dependently induced degradation of K1, assessed at 1 hrs after the UVC exposures. (b) Quantifications of the Western blot showed that UVC induced significant degradation of K1. **, $P < 0.01$. N = 12 - 15. (c, d) UVC significantly decreased the K1 levels of B 16 cells. #, $P < 0.05$ (Student *t*-test). N = 9. The data were collected from three independent experiments. (e) Western blot assays showed that administration of E-64, a broad-spectrum cysteine protease inhibitor, led to attenuation of UVC-induced K1 degradation, assessed at 1 hr after the UVC exposures. (f) Quantifications of the Western blot showed that administration with E-64 led to significant attenuation of the UVC-induced K1 degradation, assessed at 1 hr after the UVC exposures. *, $P < 0.05$; ***, $P < 0.001$. N = 4 - 6. (g) AF imaging study showed that administration of NAC led to decreases in the 0.66 J/cm^2 UVC-induced epidermal AF, assessed at 1 hrs after the UVC exposures. (h) Quantifications of the AF images showed that NAC significantly attenuated the UVC-induced epidermal AF. N = 12 - 15. **, $P < 0.01$. (i) Western blot assays showed that administration of NAC led to decreases in the 0.66 J/cm^2 UVC-induced degradation of K1, assessed at 1 hrs after the UVC exposures. (j) Quantifications of the Western blot showed that NAC significantly attenuated the UVC-induced degradation of K1,**, $P < 0.01$. N = 12 - 15. (k, l) K1 siRNA, but not K10 siRNA, dose-dependently induced early-stage (Annexin V$^+$/AAD$^-$) and late-stage apoptosis (Annexin V$^+$/AAD$^+$) as well as necrosis (Annexin V$^-$/AAD$^+$) of B16-F10 cells. *, $P < 0.05$; **, $P < 0.01$; ***, $P < 0.001$. N = 8 – 14. The data were collected from two independent

experiments. (m) K1 siRNA, but not K10 siRNA, induced increases in the DCF levels of B16-F10 cells. *, $P < 0.05$; N = 7-19. The data were collected from two independent experiments. (n) The representative figure shows that K1 siRNA, but not K10 siRNA, induced a marked increase in the ethidium levels of B16-F10 cells. N = 9. The data were collected from three independent experiments.

Figure 4. LPS and oxidative stress can induce increased green AF of the skin of C57BL/6SLAC mice' ears or B16-F10 cells, respectively. (a) Intraperitoneal injection of 0.1, 0.5 and 1 mg/kg LPS does-dependently increased the epidermal green AF of the ears, assessed at 3 days after the LPS injection. (b) Quantifications of the AF showed that 0.5 and 1 mg/kg LPS induced significant increases in the epidermal green AF of the ears. Three days after the mice were administered with 0.1, 0.5 and 1 mg/kg LPS, the epidermal green AF images of the mice' ears were taken under a two-photon fluorescence microscope. N = 6. #, $P < 0.05$; ###, $P < 0.001$ (Student *t*-test), *, $P < 0.05$; ***, $P < 0.001$. (c,d) H_2O_2 concentration-dependently increased the green AF intensity of B16-F10 cells. *, $P < 0.05$; ***, $P < 0.001$. N = 9. The data were collected from three independent experiments.

Figure 5. The green AF intensity of the skin is correlated with the risk of the CSVD patients to develop AIS. (a) The epidermal green AF intensity at both right ($R^2 = 0.9997$) and left Dorsal Index Fingers ($R^2 = 0.9884$) was highly correlated with the risk levels of the CSVD patients to develop AIS. #, $P < 0.05$ (Student *t*-test). The number of subjects for the healthy group, the group of the CSVD patients with low-risk of developing AIS, and the

group of CSVD patients with high-risk of developing AIS was 37, 100 and 61, respectively. (b) The epidermal green AF intensity at both right (R^2 = 0.9530) and left (R^2 = 0.9979) Ventroforefinger was highly correlated with the risk levels of the CSVD patients to develop AIS. *, $P < 0.05$; **, $P < 0.01$. The number of subjects for the healthy group, the group of the CSVD patients with low-risk of developing AIS, and the group of CSVD patients with high-risk of developing AIS was 37, 100 and 61, respectively. (c, d) There was marked variability in the basal AF intensity of the various regions of the skin of healthy people. *, $P < 0.05$; **, $P < 0.01$; ***, $P < 0.001$. N = 37. (e, f) There was marked variability in the basal AF intensity of the various regions of the skin of the CSVD patients *, $P < 0.05$; **, $P < 0.01$; ***, $P < 0.001$. N = 60 - 61. (g, h) There was marked variability in the basal AF intensity of the various regions of the skin of AIS patients. *, $P < 0.05$; **, $P < 0.01$; ***, $P < 0.001$. N = 64 - 68.

Figure 6. Diagrammatic presentation of the 'Pattern of Autofluorescence Theory for Organ Injury'. The dotted line denotes the pathway that requires further demonstration.

Figure 7. Diagrammatic presentation of the 'Keratin Degradation-Mediated Skin Damage Theory for UV-Induced Skin Damage'.

Legends of Supplemental Figures:

Supplemental Figure 1. H&E staining of the skin of C57BL/6SLAC mice's ears. H&E staining of the skin showed that the thickness of the epidermis is approximately 25 - 30 μm, while the thickness of the stratum corneum is less that 3 μm. Scale bar = 25 μm. N = 6.

Supplemental Figure 2. Both UVB and UVA can dose-dependently induce significant increases in the epidermal AF of C57BL/6SLAC mice's ears. (a) Exposures of the ears of C57BL/6SLAC mice to 1.3 and 2.6 J/cm^2 UVB led to increases in the green AF, assessed at 24 hrs after the exposures. Scale bar = 20 μm. (b) Quantifications of the AF showed that each dose of UVB induced significant increases in the skin AF of the ears of C57BL/6SLAC mice. *, $P < 0.05$; **, $P < 0.01$. N = 10 – 13. (c) Exposures of the ears of C57BL/6SLAC mice to UVA at the dosage of 5.4 J/cm^2 led to increases in the green AF, assessed at 24 hrs after the exposures. Scale bar = 20 μm. (d) Quantifications of the AF showed that exposures of the ears of C57BL/6SLAC mice to UVA at the dosage of 5.4 J/cm^2 led to a significant increase in the green AF, assessed at 24 hrs after the exposures. *, $P < 0.05$. N = 11-15. (e) The spectra of the UVC-, UVB- and UVA-induced skin's AF of C57BL/6SLAC mice's ears were similar. Three C57BL/6SLAC mice were used for determination of each of the spectrum of the UVC-, UVB- and UVA-induced AF. Each line in the figure is the representative spectrum of one mouse that was exposed to certain type of UV radiation.

Supplemental Figure 3. UVC produced a significant decrease in the FAD level of the

skin of C57BL/6SLAC mice's ears 1 hr after the UVC exposures. ##, $P < 0.01$ (Student *t*-test). N = 6.

Supplemental Figure 4. TEM study on the ear's epidermis of C57BL/6SLAC mice. TEM study on the ear's epidermis of C57BL/6SLAC mice showed polyhedral structures and dense bundles in the layers that are 10 – 20 μm from the outer layer of the epidermis.

Supplemental Figure 5. Immunostaining of the skin of C57BL/6SLAC mice's ears using anti-K1 antibody showed polyhedral structure of the K1-positive regions. N = 6.

Supplemental Figure 6. There was no significant difference among the FAD levels in the ears and the back of C57BL/6SLAC mice and nude mice. N = 6.

Supplemental Figure 7. The laser treatment led to a marked increase in the fluorescent signal of Cy5-labeled siRNA inside the skin. N = 3.

Supplemental Figures 8. E-64 led to significant attenuation of UVC-induced K1 degradation. (A) Western blot assays showed that administration of E-64, a broad-spectrum cysteine protease inhibitor, led to attenuation of UVC-induced K1 degradation, assessed at 1 hr after the UVC exposures. (B) Quantifications of the Western blot showed that administration with E-64 led to significant attenuation of UVC-induced K1 degradation, assessed at 1 hr after the UVC exposures. *, $P < 0.05$; ***, $P < 0.001$. N = 4 - 6.

Supplemental Figures 9. (a) Western blot assays showed a selective and remarkable increase in the K1 monomers in the B16-F10 cells overexpressing Flagged-K1 with Flag at its C-terminus, which was markedly decreased by UVC exposures. N = 3. (c) There was a marked increase in UVC-induced green AF in the B16-F10 cells overexpressing Flagged-K1. N = 9. Data were collected from three independent experiments.

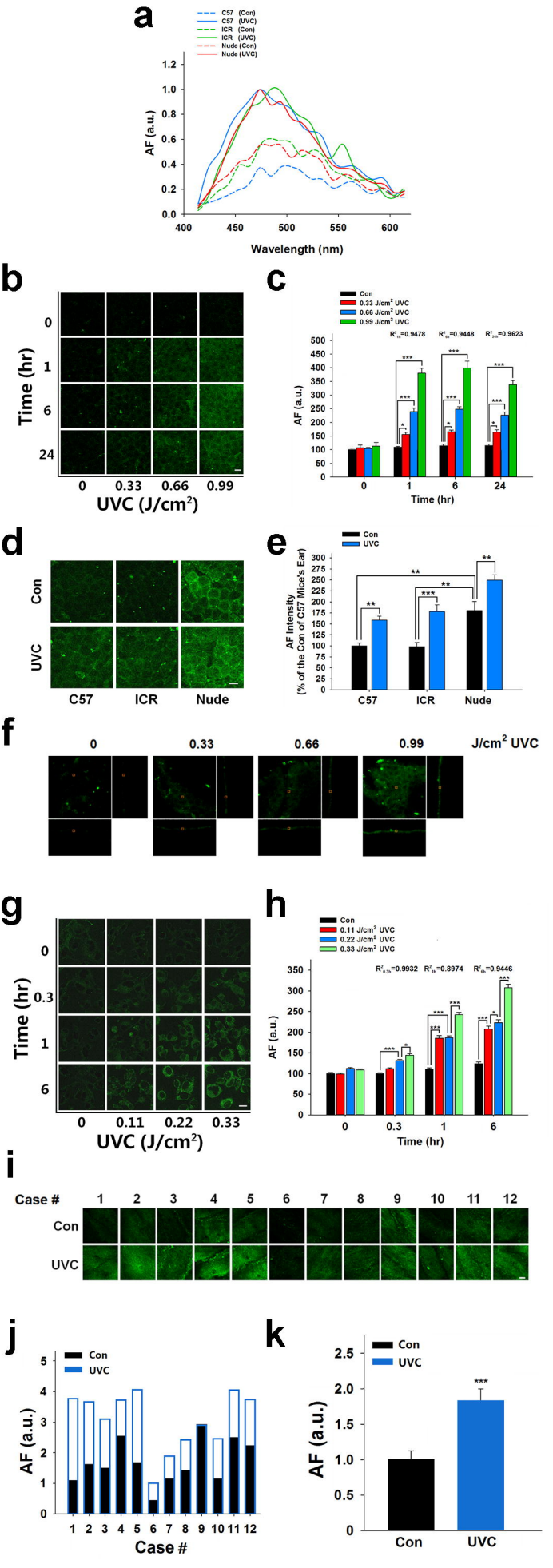
a
C57 (Con)
C57 (UVC)
ICR (Con)
ICR (UVC)
Nude (Con)
Nude (UVC)
AF (a.u.)
Wavelength (nm)
b
Time (hr)
0
1
6
24
0
0.33
0.66
0.99
UVC (J/cm²)
c
Con
0.33 J/cm² UVC
0.66 J/cm² UVC
0.99 J/cm² UVC
AF (a.u.)
Time (hr)
d
Con
UVC
C57
ICR
Nude
e
Con
UVC
AF Intensity
(% of the Con of C57 Mice's Ear)
C57
ICR
Nude
f
0
0.33
0.66
0.99
J/cm² UVC
g
Time (hr)
0
0.3
1
6
0
0.11
0.22
0.33
UVC (J/cm²)
h
Con
0.11 J/cm² UVC
0.22 J/cm² UVC
0.33 J/cm² UVC
AF (a.u.)
Time (hr)
i
Case #
1
2
3
4
5
6
7
8
9
10
11
12
Con
UVC
j
Con
UVC
AF (a.u.)
Case #
k
Con
UVC
AF (a.u.)
Con
UVC

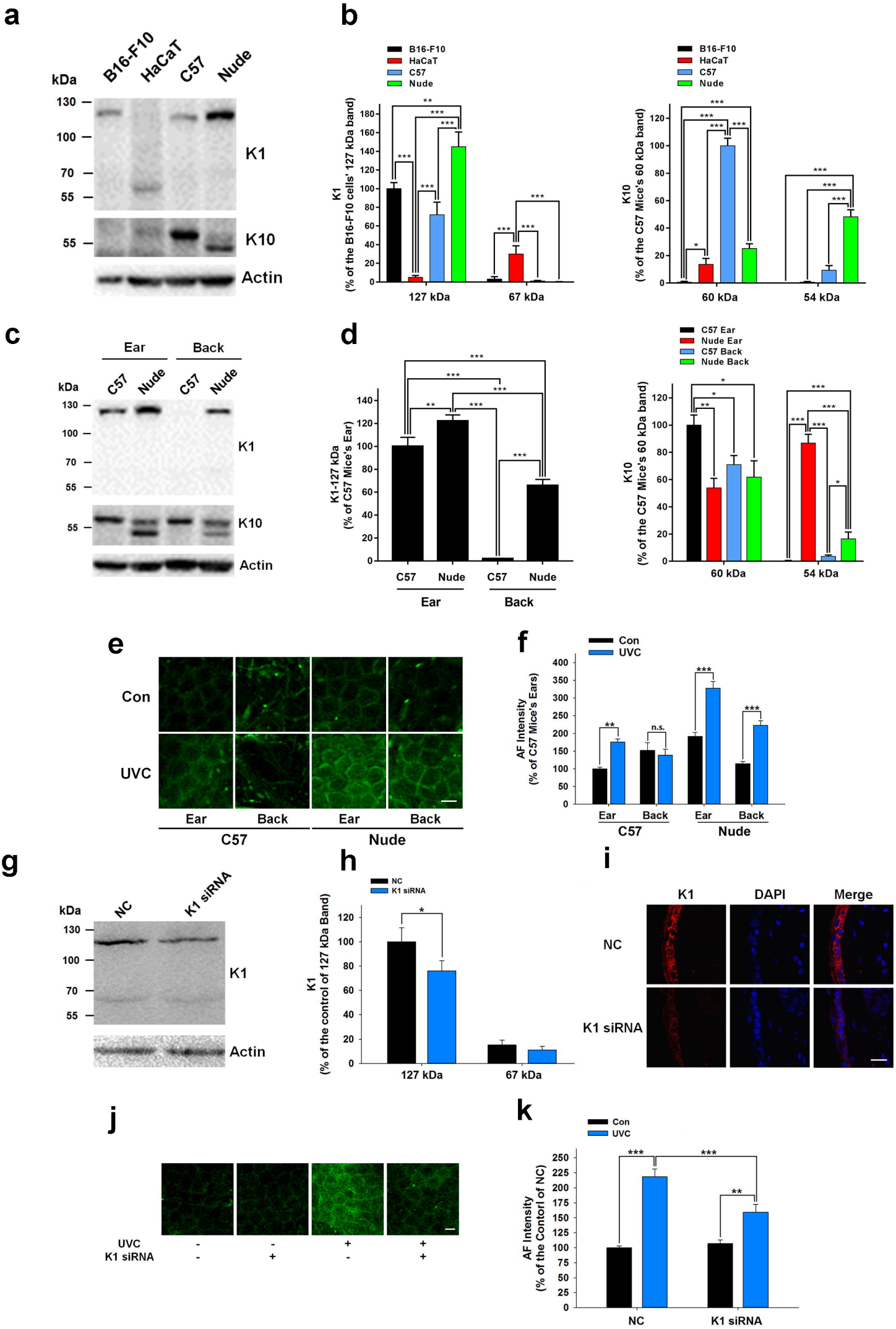
a
kDa
B16-F10
HaCaT
C57
Nude
130
100
70
55
K1
55
K10
Actin
b
B16-F10
HaCaT
C57
Nude
K1
(% of the B16-F10 cells' 127 kDa band)
127 kDa
67 kDa
K10
(% of the C57 Mice's 60 kDa band)
60 kDa
54 kDa
c
Ear
Back
C57
Nude
C57
Nude
kDa
130
100
70
55
K1
55
K10
Actin
d
K1-127 kDa
(% of C57 Mice's Ear)
C57
Nude
C57
Nude
Ear
Back
C57 Ear
Nude Ear
C57 Back
Nude Back
K10
(% of the C57 Mice's 60 kDa band)
60 kDa
54 kDa
e
Con
UVC
Ear
Back
Ear
Back
C57
Nude
f
Con
UVC
AF Intensity
(% of C57 Mice's Ears)
n.s.
Ear
Back
Ear
Back
C57
Nude
g
kDa
NC
K1 siRNA
130
100
70
55
K1
Actin
h
NC
K1 siRNA
K1
(% of the control of 127 kDa Band)
127 kDa
67 kDa
i
K1
DAPI
Merge
NC
K1 siRNA
j
UVC
K1 siRNA
k
Con
UVC
AF Intensity
(% of the Contorl of NC)
NC
K1 siRNA

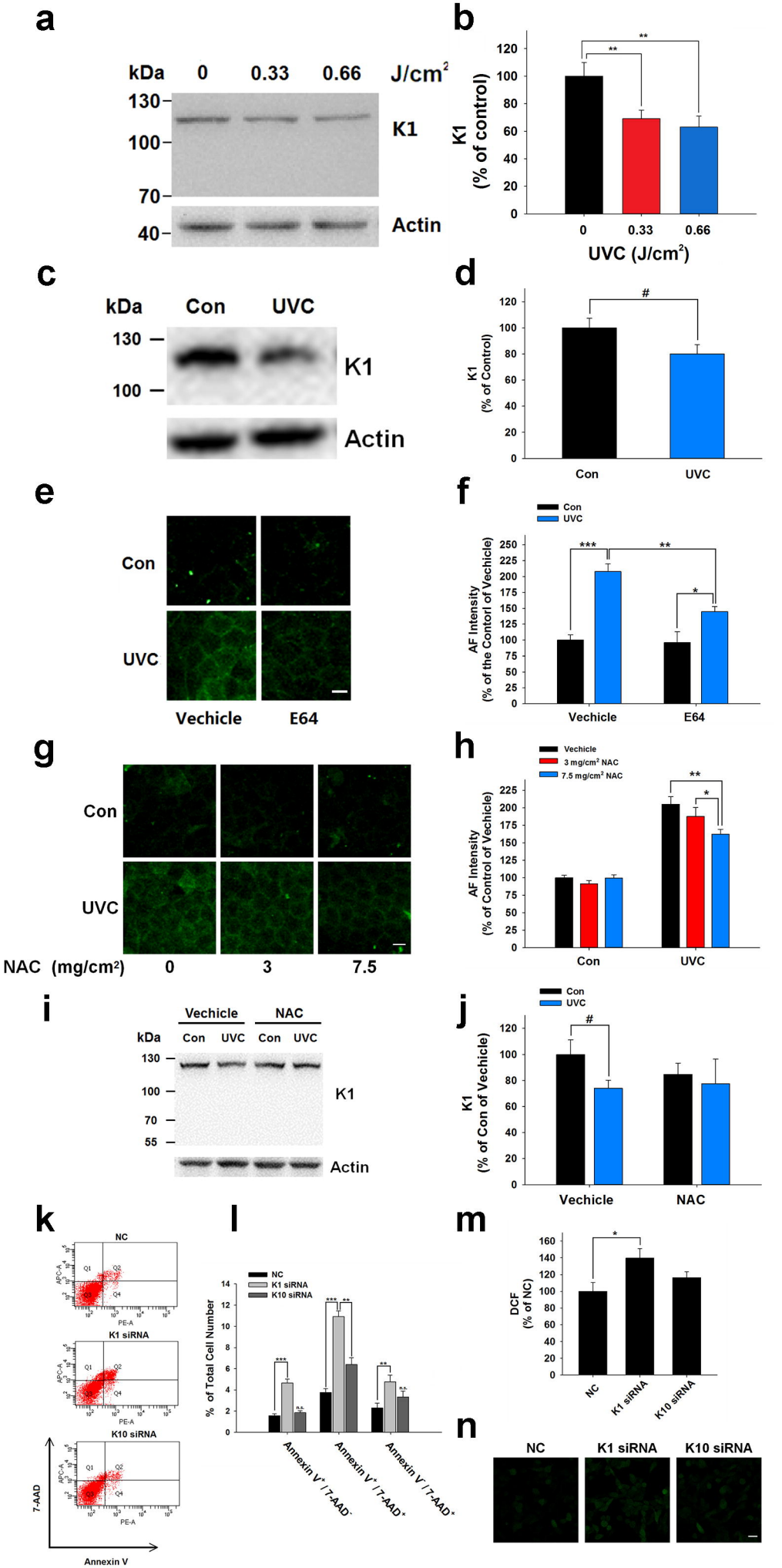
a
kDa
0
0.33
0.66
J/cm²
130
100
70
40
K1
Actin
b
K1 (% of control)
UVC (J/cm²)
c
kDa
Con
UVC
130
100
K1
Actin
d
K1 (% of Control)
Con
UVC
e
Con
UVC
Vechicle
E64
f
Con
UVC
AF Intensity (% of the Contorl of Vechicle)
Vechicle
E64
g
Con
UVC
NAC (mg/cm²)
0
3
7.5
h
Vechicle
3 mg/cm² NAC
7.5 mg/cm² NAC
AF Intensity (% of Control of Vechicle)
Con
UVC
i
Vechicle
NAC
kDa
Con
UVC
Con
UVC
130
100
70
55
K1
Actin
j
Con
UVC
K1 (% of Con of Vechicle)
Vechicle
NAC
k
NC
K1 siRNA
K10 siRNA
PE-A
APC-A
Q1
Q2
Q4
7-AAD
Annexin V
l
NC
K1 siRNA
K10 siRNA
% of Total Cell Number
Annexin V⁺ / 7-AAD⁻
Annexin V⁺ / 7-AAD⁺
Annexin V⁻ / 7-AAD⁺
m
DCF (% of NC)
NC
K1 siRNA
K10 siRNA
n
NC
K1 siRNA
K10 siRNA

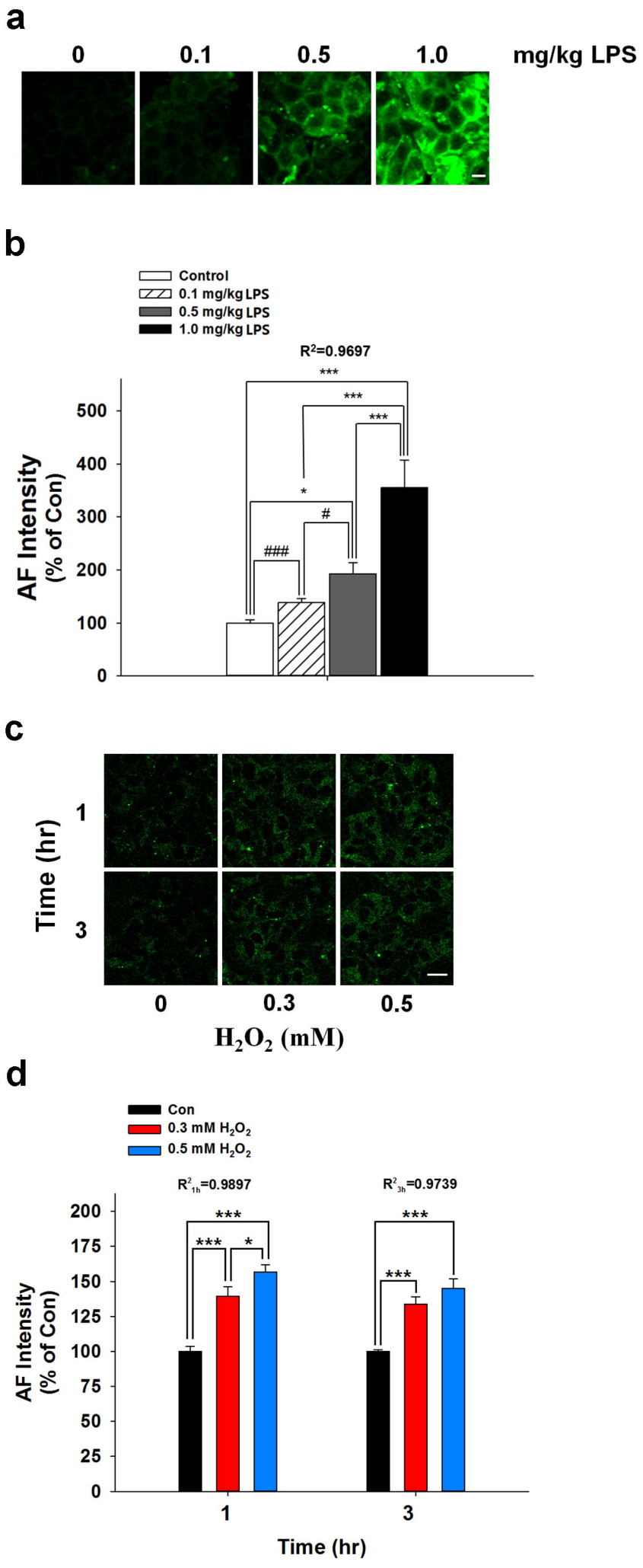
a
0
0.1
0.5
1.0
mg/kg LPS
b
Control
0.1 mg/kg LPS
0.5 mg/kg LPS
1.0 mg/kg LPS
R2=0.9697
AF Intensity
(% of Con)
0
100
200
300
400
500
***
***
***
*
#
###
c
Time (hr)
1
3
0
0.3
0.5
H2O2 (mM)
d
Con
0.3 mM H2O2
0.5 mM H2O2
R21h=0.9897
R23h=0.9739
AF Intensity
(% of Con)
0
25
50
75
100
125
150
175
200
***
***
*
***
***
1
3
Time (hr)

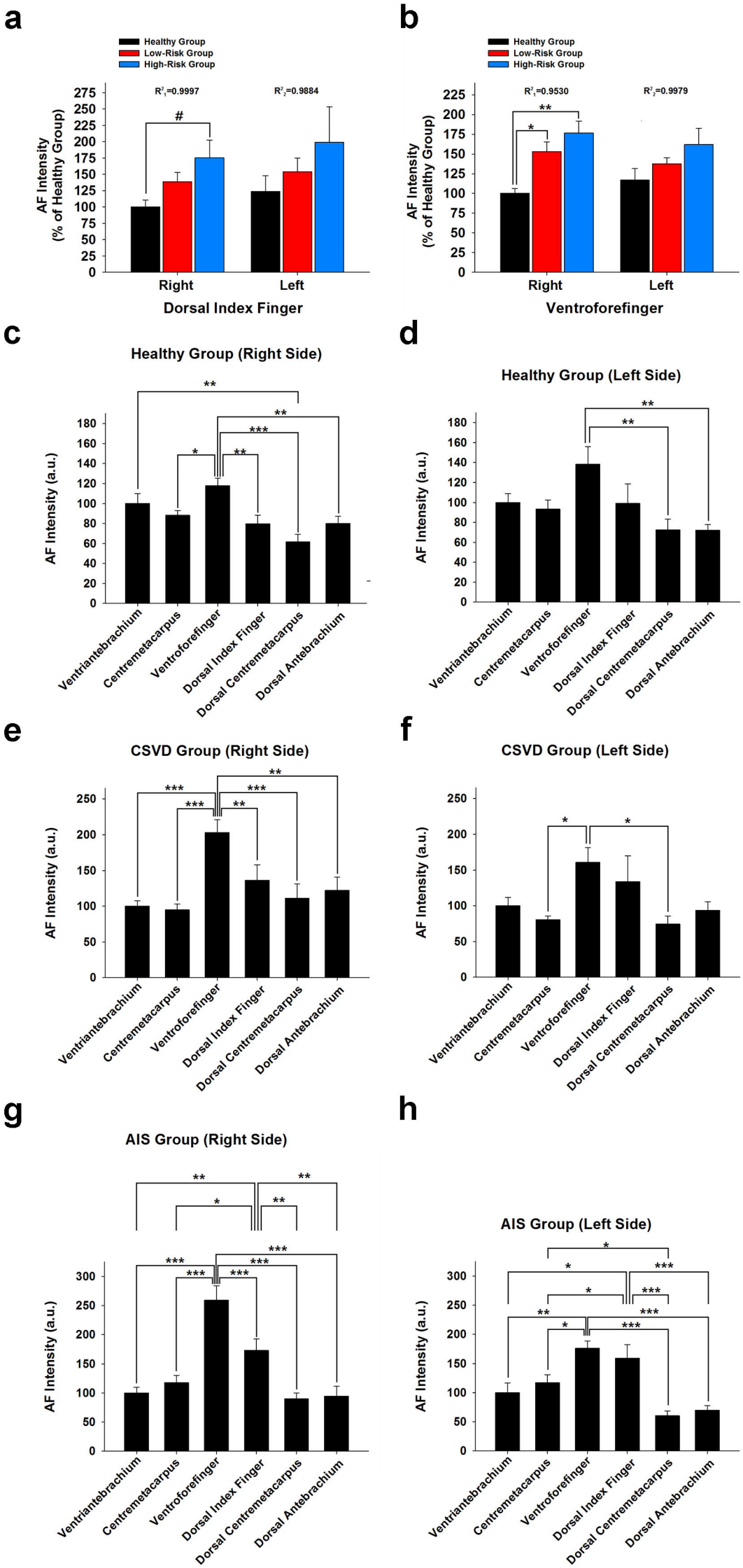
a
Healthy Group
Low-Risk Group
High-Risk Group
R^2_1=0.9997
R^2_2=0.9884
#
AF Intensity (% of Healthy Group)
Right
Left
Dorsal Index Finger
b
R^2_1=0.9530
R^2_2=0.9979
**
*
Ventroforefinger
c
Healthy Group (Right Side)
AF Intensity (a.u.)
Ventriantebrachium
Centremetacarpus
Ventroforefinger
Dorsal Index Finger
Dorsal Centremetacarpus
Dorsal Antebrachium
d
Healthy Group (Left Side)
e
CSVD Group (Right Side)
***
f
CSVD Group (Left Side)
g
AIS Group (Right Side)
h
AIS Group (Left Side)

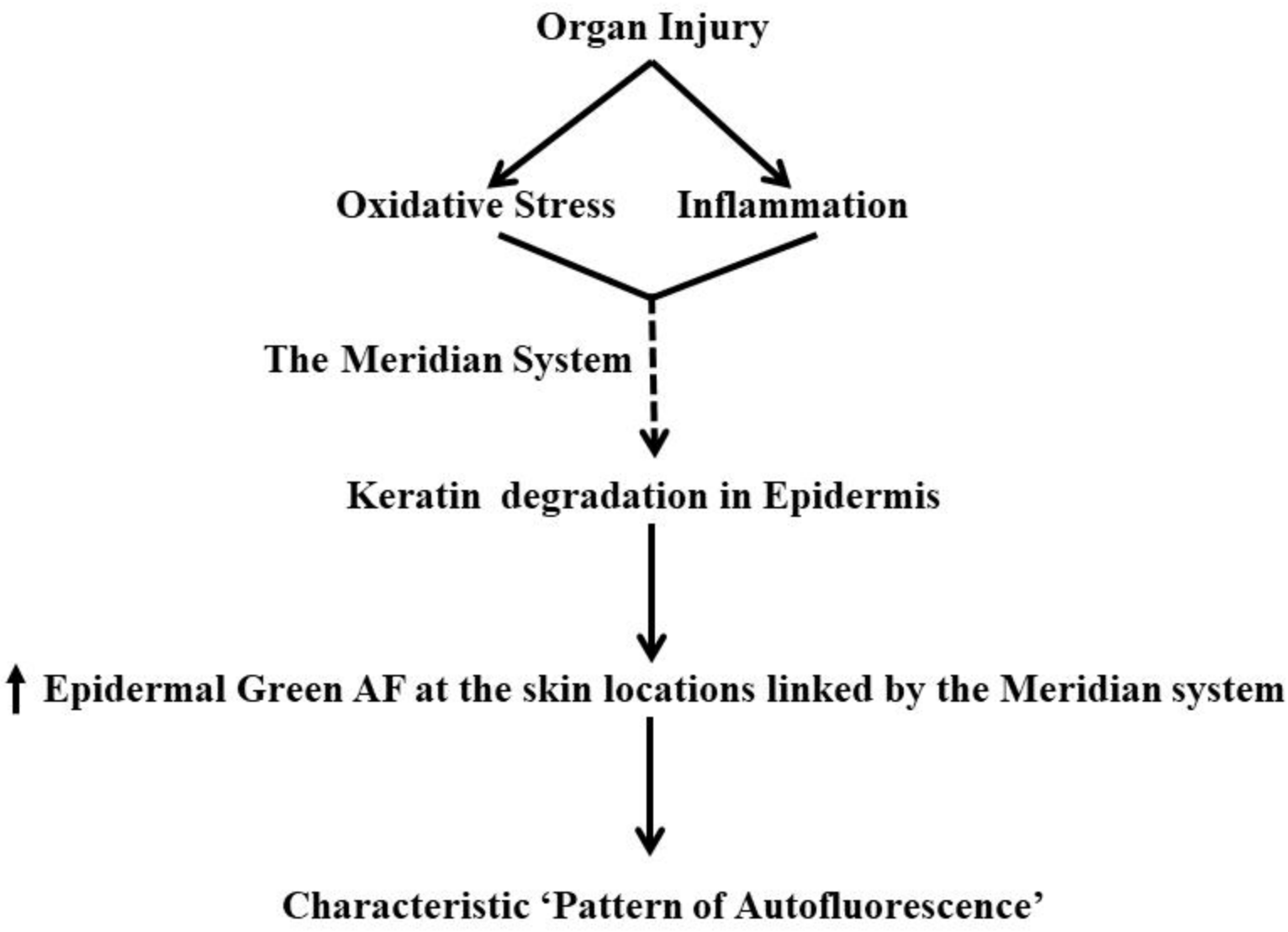
Organ Injury
Oxidative Stress
Inflammation
The Meridian System
Keratin degradation in Epidermis
↑ Epidermal Green AF at the skin locations linked by the Meridian system
Characteristic 'Pattern of Autofluorescence'

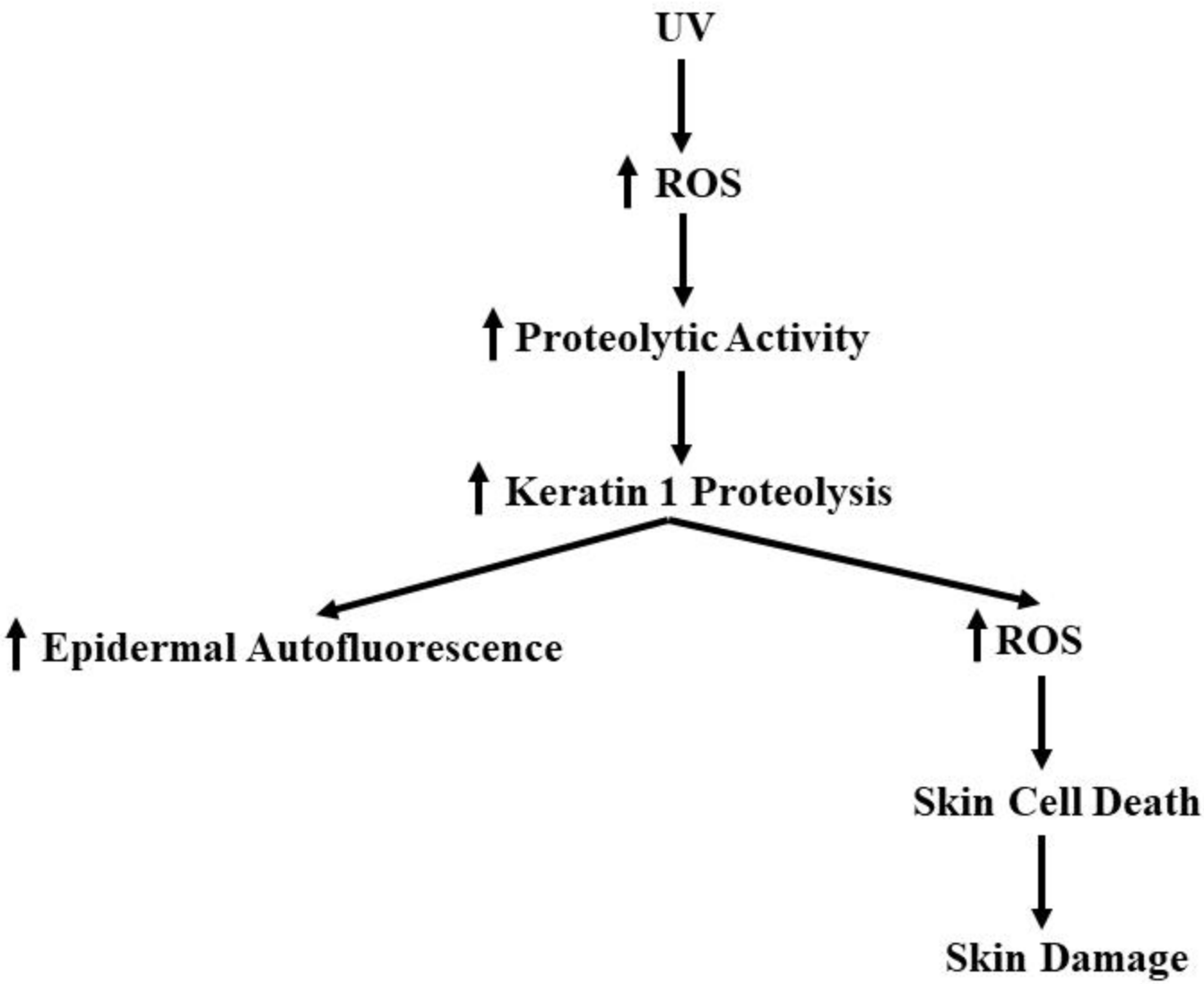
UV
↑ ROS
↑ Proteolytic Activity
↑ Keratin 1 Proteolysis
↑ Epidermal Autofluorescence
↑ ROS
Skin Cell Death
Skin Damage